NANO LETTERS

Letter

pubs.acs.org/NanoLett

Enhanced Magnetoresistance in Molecular Junctions by Geometrical Optimization of Spin-Selective Orbital Hybridization

David Rakhmilevitch,[†] Soumyajit Sarkar,[‡] Ora Bitton,[§] Leeor Kronik,[‡] and Oren Tal*[,†]

[†]Department of Chemical Physics, [‡]Department of Materials and Interfaces, and [§]Department of Chemical Research Support, Weizmann Institute of Science, Rehovot, Israel

Supporting Information

ABSTRACT: Molecular junctions based on ferromagnetic electrodes allow the study of electronic spin transport near the limit of spintronics miniaturization. However, these junctions reveal moderate magnetoresistance that is sensitive to the orbital structure at their ferromagnet−molecule interfaces. The key structural parameters that should be controlled in order to gain high magnetoresistance have not been established, despite their importance for efficient manipulation of spin transport at the nanoscale. Here, we show that single-molecule junctions based on nickel electrodes and benzene molecules can yield a significant anisotropic magnetoresistance of up to ∼200% near the conductance quantum G_0. The measured magnetoresistance is mechanically tuned by changing the distance between the electrodes, revealing a nonmonotonic response to junction elongation. These findings are ascribed with the aid of first-principles calculations to variations in the metal−molecule orientation that can be adjusted to obtain highly spin-selective orbital hybridization. Our results demonstrate the important role of geometrical considerations in determining the spin transport properties of metal−molecule interfaces.

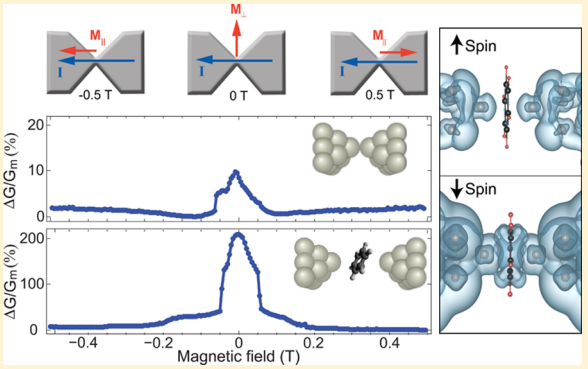

KEYWORDS: *Spintronics, spinterface, molecular electronics, magnetoresistance, molecular junction, spin transport*

Spintronics has a large impact on daily life, being the backbone of computer hard drives.[1] The reduction in size of spintronic elements is of central importance for efficient information processing, as well as for demonstrating intriguing physical phenomena.[2−6] In this respect, magnetoresistance measurements across molecular junctions provide a useful test-bed for spin transport at the nanoscale.[7] Previous studies showed that magnetoresistance in molecular junctions is sensitive to the orbital structure at the metal−molecule interfaces.[8−10] However, the structural aspects that should be considered in order to gain optimal magnetoresistance enhancement have not been studied. This information is necessary in order to develop a practical methodology for controlled spin transport across metal−molecule interfaces in a variety of nanoscale molecular junctions and organic spintronic devices. Here, we show that anisotropic magnetoresistance (AMR) in molecular junctions can be enhanced by more than an order of magnitude with respect to the corresponding bare atomic junctions, while mechanical modifications of the junction efficiently tune the obtained magnetoresistance. With the aid of first-principle calculations, these effects are explained by spin-selective orbital hybridization that can be optimized by tuning the relative orientation between the metal electrodes and the molecule. Our findings shed light on the structural and geometrical conditions at metal−molecule interfaces that are required for optimal magnetoresistance.

The mechanism underlying AMR in the bulk is anisotropic scattering of electrons as a result of spin−orbit interaction, which depends on the relative orientation of the magnetization and the electronic current. Generally, stronger scattering is expected for current aligned with the conductor magnetization, leading to higher resistivity in comparison to current perpendicular to the magnetization (Figure 1, bottom left inset). The change in resistance for bulk ferromagnetic metals is small and does not exceed 5%.[11] Interestingly, when the size of a ferromagnet is reduced to the atomic-scale, the AMR response is enhanced to 10−15%.[12,13] This enhancement was ascribed to the high sensitivity of the local electronic structure at the atomic constriction to the magnetization direction, resulting in large variations in the electronic transmission.[14−16] While larger than the bulk response, AMR in atomic-scale devices based on metallic ferromagnetic electrodes is limited by their moderate injection of spin current. The conductance of these metals is dominated by the insignificantly spin-polarized sp bands rather than by the spin-polarized d bands, resulting in moderate conductance variations in response to magnetic manipulations.[11] The limited spin injection from ferromagnetic metals is a general drawback, leading to the incorporation of

Received: November 16, 2015
Revised: February 4, 2016
Published: February 29, 2016

DOI: 10.1021/acs.nanolett.5b04674
Nano Lett. 2016, 16, 1741−1745

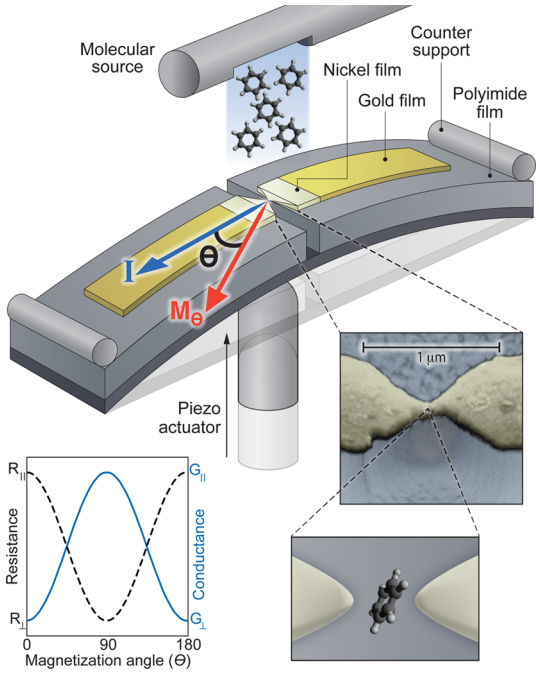

Figure 1. Schematic description of the measurement setup. The sample is composed of lithographically-defined gold electrodes, connected by a microscale ferromagnetic Ni constriction. The central panel depicts a scanning electron microscope image of the constriction and the suspended bridge. A three-point bending mechanism is used to controllably break the constriction so as to form atomic and tunnel junctions. Benzene molecules are introduced to the junctions via a molecular source in order to form molecular junctions (schematically depicted in the bottom right panel). By applying an external magnetic field the relative angle (θ) between the magnetization of the junction and the current across it is changed, affecting the conductance (or resistance) as schematically illustrated in the bottom left inset for a bulk contact.

sophisticated structures and exotic materials[17,18] in order to increase the magnetoresistance and therefore the sensitivity of spintronic devices. This limitation can be confronted by taking advantage of the chemical binding between π-conjugated molecules and ferromagnetic metals to promote transport via the frontier spin-polarized d-orbitals of ferromagnetic electrodes.[9,19,20] Yet, having such a spin-selective orbital hybridization is only a prerequisite and geometrical aspects should be taken into consideration.

We use a break-junction setup at cryogenic temperatures (5.9 K) to study AMR in nanoscale contacts, as well as in atomic and molecular junctions using the same sample. This approach allows for a reliable comparison between the AMR properties of the three systems. The samples are made of two gold leads connected by a microscale ferromagnetic nickel (Ni) section (Figure 1). The metallic structure is firmly attached to a bendable substrate, excluding a nanoscale segment at the center of the Ni constriction. With the aid of a three-point bending mechanism, the suspended Ni segment is stretched and broken in cryogenic vacuum, exposing two ultraclean Ni apexes. The distance between these electrodes can be adjusted with sub-angstrom resolution to repeatedly form single-atom junctions with different atomic tip configurations. Molecular junctions are obtained by introducing benzene molecules in situ via a molecular source. Our sample design is optimized to efficiently suppress undesired magnetostrictive effects that can contribute to the measured magnetoresistance by changing the distance between the electrodes. This is achieved by minimizing the ferromagnetic section of the junction and in particular the freely suspended region.[21] The negligible role of magnetostriction is verified by the absence of systematic changes in magnetoresistance in control experiments performed on the bare Ni junctions at the onset of tunneling conductance. Further details can be found in the Supporting Information.

AMR can be measured by changing the direction of sample magnetization with respect to the current with the aid of a rotating magnetic field. Relevant results based on this measurement technique are presented in the Supporting Information for atomic and molecular junctions. However, when measuring atomic-scale junctions, this approach promotes abrupt conductance variations that may stem (among other possibilities) from local atomic and molecular rearrangements induced by the rotating magnetic field,[22] rather than from intrinsic AMR. To avoid ambiguity, we adopted a simpler yet well-established measurement scheme.[23,24] We first analyzed the conductance response to magnetic field sweeps along the three principal axes of our junctions and identified that near zero magnetic field the junctions are spontaneously magnetized perpendicular to the junction axis and in its plane[25] (as discussed thoroughly in the Supporting Information). Then, the conductance was measured while the magnetic field is swept along the sample axis (Figure 2a). The magnetization of

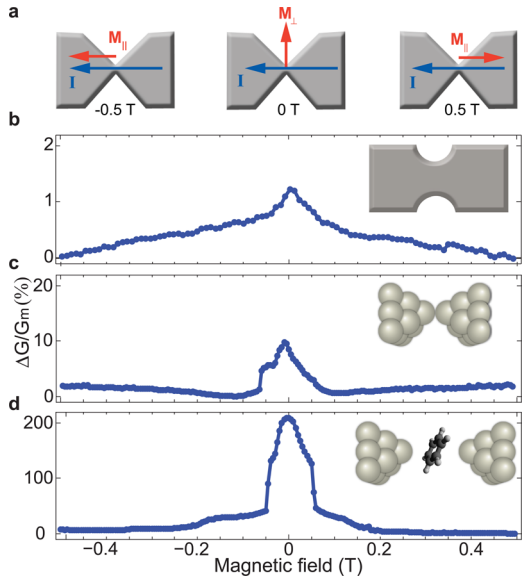

Figure 2. (a) Schematic description of the junction magnetization during a sweep of magnetic field along the sample axis. AMR measured on (b) a nanoscale contact ($G_m = 98G_0$), (c) a Ni atomic junction ($G_m = 1.36G_0$), and (d) a Ni/benzene molecular junction ($G_m = 0.42G_0$). The similar trend of the relative conductance for the atomic and molecular junctions suggests that the easy axis for magnetization is the same in both cases.

the sample is initially aligned antiparallel to the current by applying a magnetic field of 0.5 T in this direction, leading to a low conductance. As the magnetic field is reduced to zero the magnetization is spontaneously aligned perpendicular to the current, resulting in a higher conductance. Finally, when the magnetic field is increased in the opposite direction the magnetization is aligned in parallel to the current. This scheme yields fairly smooth conductance variations as a function of

DOI: 10.1021/acs.nanolett.5b04674
Nano Lett. 2016, 16, 1741−1745

magnetic field, for both atomic and molecular junctions, indicating the lack of abrupt atomic and molecular rearrangements in the junction constriction.

In atomic-scale transport measurements, it is customary to focus on conductance rather than resistance. Therefore, the AMR response is defined as $\Delta G/G_m = (G_{\parallel} - G_{\perp})/G_{\parallel} = (R_{\perp} - R_{\parallel})/R_{\perp}$ where G_i and R_i ($i = \parallel, \perp$) are the conductance and resistance parallel or perpendicular to the current direction and $G_m = G_{\parallel}$ is the minimal conductance. As a first step, we focus on the AMR response of a Ni nanoscale contact. In this regime, near zero magnetic field there are multiple magnetic domains in the vicinity of the contact and the magnetic field acts to align them with the junction axis. Figure 2b presents the AMR ratio as a function of magnetic field for a nanoscale contact with a zero-bias differential conductance of 98.0 G_0 ($G_0 \cong 1/12.9\text{K}\ \Omega$ is the conductance quantum). An AMR ratio of 1.23% is obtained, which is in agreement with the typical AMR found for bulk Ni.[11] In order to analyze the AMR response of atomic junctions, the junction was partially broken in a controllable fashion while measuring the conductance. During this process the number of atoms in the cross-section of the Ni constriction was gradually reduced up to a single-atom contact that is characterized by a typical conductance of 1.2−1.4 G_0.[26,27] Figure 2c shows that the AMR response is increased to 9.8% when an atomic junction is formed. Similar AMR enhancement was reported previously for atomic-scale junctions[12,13] and was attributed to the enhanced sensitivity of conductance across an atomic-scale constriction to magnetization-induced variations in the local density of states, or to a possible enhancement of spin−orbit interaction due to the low atomic-coordination.[14−16] Further elongation of the junction resulted in breaking of the contact and formation of a tunnel junction (see Supporting Information).

In order to study the AMR response of a molecular junction the examined atomic junction was further elongated until it was broken. At this point, benzene molecules were introduced into the junction by sublimation from a molecular source and the interelectrode separation was adjusted to form a molecular junction. The presence of a molecule in the junction was initially verified for each junction realization by measuring a stable conductance value smaller than the typical conductance of bare Ni atomic junctions. Further verification was obtained by detecting the molecular signature of vibration activation in the conductance of the junction (see Supporting Information). Figure 2d presents an AMR measurement taken after the formation of a molecular junction. The AMR response of the molecular junction reaches 208%, more than 1 order of magnitude higher than the AMR obtained for the corresponding atomic Ni junction (see Supporting Information for statistical data). This maximal AMR response is higher than previously reported magnetoresistance ratios found for single molecule junctions.[9,10,28−30]

The structure of molecular junctions evolves when the interelectrode distance is increased.[31] To characterize the effect of structural modifications on magneto-transport, we studied the response of the AMR ratio to junction elongation. The interelectrode separation was increased in sub-angstrom sequential steps of 0.1 Å, while the conductance and AMR response were measured at each step. As can be seen in Figure 3a, the conductance is monotonically reduced when the junction is elongated. In contrast, the AMR is first enhanced, reaching an optimal value at $G_m \sim 0.4G_0$ (Figure 3b), and decreases afterward. This behavior indicates that the AMR ratio

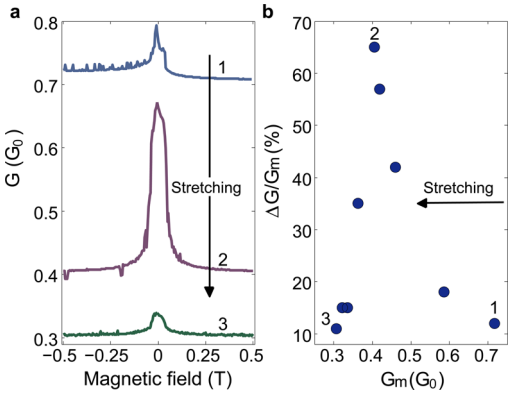

Figure 3. (a) Selected magnetoconductance curves for different junction elongations. (b) AMR ratio for the entire stretching sequence, partially shown in (a), as a function of G_m; the decrease in G_m is due to a monotonic increase in electrode separation (further details appear in the Supporting Information).

is optimal in a certain molecular junction configuration, allowing mechanical tunability of the AMR effect. We note that the nonmonotonic AMR response is consistent with the negligible role of magnetostriction in our design. This undesired effect is expected to yield monotonically increasing magnetoresistance as the conductance is reduced by stretching toward the tunneling regime.

To shed light on the origin of the high AMR in our single molecule junctions, as well as its evolution during junction elongation we performed density functional theory (DFT) based first-principles calculations (see Supporting Information). We note that related transport calculations were recently reported for a model system of a Ni-benzene junction.[32] Figure 4a shows the spin-resolved projected density of states on the π (PDOS^{π}) and σ (PDOS^{σ}) benzene orbitals, at an interelectrode distance of 7.2 Å for which the junction has a minimum total energy (see Supporting Information). At the Fermi energy, the energy relevant for transport, PDOS^{π} is considerably larger than PDOS^{σ}. Moreover, in contrast to PDOS^{σ}, the different PDOS^{π} for the spin up and down channels indicate a clear spin-polarization near the Fermi energy. Because the isolated molecule has no magnetic moment and charge transfer between the molecule and the electrodes is negligible (see Supporting Information), the observed spin-polarization should stem from hybridization with the magnetic electrodes.[20,33,34]

A better understanding of this effect can be gained by looking at the corresponding real-space plot of the spin-resolved charge density around the Fermi energy (Figure 4b). For the spin down channel, an efficient hybridization between the frontier d-orbitals of the Ni electrodes and the π-orbitals of the molecule is clearly visible. This is in clear contrast to the spin up channel, showing minor orbital hybridization between the molecule and the electrodes. The significantly different hybridization for the spin up and spin down channels leads to high spin polarization (further details appear in the Supporting Information). Similar selective π−d hybridization was revealed experimentally for benzene molecules adsorbed on Ni surfaces.[35] Because of anisotropic spin−orbit coupling in ferromagnetic atomic-scale junctions, spin-polarized states are shifted with respect to the Fermi energy in response to changes in the magnetization direction.[14−16,32] As a result, the dominant role of the spin-polarized π−d hybridized states at the Fermi energy is expected to enhance the AMR response of the molecular junction.

DOI: 10.1021/acs.nanolett.5b04674
Nano Lett. 2016, 16, 1741−1745

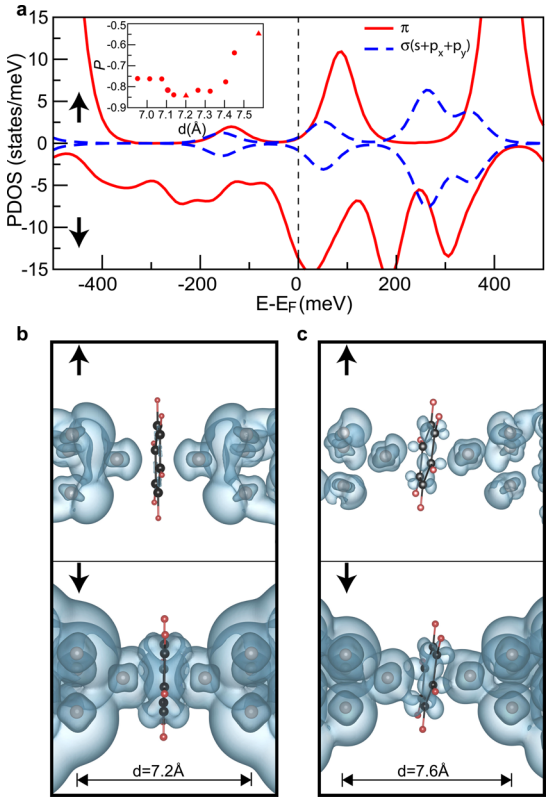

Figure 4. (a) Calculated density of states projected on the π- (solid, red) and σ- (dashed, blue) orbitals of the benzene molecule for an interelectrode separation of 7.2 Å. Inset: calculated P for different interelectrode separation, d. The values of P for interelectrode distances of 7.2 and 7.6 Å, discussed in the text, are marked with triangles. (b,c) Spin-resolved charge density plots for an energy window of 100 meV around the Fermi energy for two junction configurations with an interelectrode distance of 7.2 Å (b) and 7.6 Å (c), respectively.

The observed tunable AMR can be explained by the directionality of d-orbitals in space, dictating that the π–d hybridization is sensitive to variations in the mutual orientation of these orbitals.[31,36] The degree of spin polarization of PDOS$^{\pi}$ at the Fermi energy can indicate the relevant spin selectivity for transport. This quantity is defined as $P = \frac{\mathrm{PDOS}^{\pi}_{\uparrow}(E_F) - \mathrm{PDOS}^{\pi}_{\downarrow}(E_F)}{\mathrm{PDOS}^{\pi}_{\uparrow}(E_F) + \mathrm{PDOS}^{\pi}_{\downarrow}(E_F)}$ and it is presented in the inset of Figure 4a as a function of electrode separation. Similar to the measured AMR, the spin polarization P is clearly subjected to nonmonotonic variations as a function of junction elongation. Comparison between the spin-resolved charge density plots for compact (Figure 4b) and extended (Figure 4c) junction configurations reveals that the molecule tilts with respect to the electrode axis as a result of junction elongation. In the extended configuration, the overall hybridization between the molecule and the electrode frontier orbitals is reduced, and non-negligible π–d hybridization is now found for both spin up and spin down electrons, resulting in the observed decrease in spin polarization. For relatively compact junction configurations with measured conductance above $0.4G_0$ (Figure 3b), the reduction in P indicates a less dominant contribution of spin-polarized states to the conductance and hence moderate AMR. Beyond this effect, for close enough electrodes some reduction of AMR may result from poorly spin-polarized tunneling conductance between the Ni apexes. This background conductance, which is dominated by the Ni frontier s-orbitals, is rather insensitive to magnetization variations.[32] The exemplified structural flexibility of the molecular junction can therefore be used to modify the orbital hybridization in the junction and optimize the AMR response.

To conclude, significantly high and tunable AMR was demonstrated in Ni/benzene molecular junctions. Our analysis indicate an optimal molecular orientation with respect to the ferromagnetic metal electrodes, in which a maximal AMR is achieved due to efficient spin-selective orbital hybridization. These findings demonstrate the importance of geometrical considerations in determining the spin transport properties at metal–molecule interfaces and open the door for controlled magnetoresistance by geometrical modifications at such interfaces.

■ ASSOCIATED CONTENT

Supporting Information

The Supporting Information is available free of charge on the ACS Publications website at DOI: 10.1021/acs.nanolett.5b04674.

Device fabrication and molecule insertion schemes; the role of magneto-elastic effects in our junctions; AMR measurements in a rotating magnetic field; determination of the easy-axis in our junctions; establishing transport through the molecule using inelastic electron spectroscopy; the effects of variable molecular configurations; description of computational methodology and details of the model system; analysis of charge transfer between the molecule and the electrodes; and additional real-space spin-resolved charge density plots. (PDF)

■ AUTHOR INFORMATION

Corresponding Author

*E-mail: oren.tal@weizmann.ac.il.

Author Contributions

D.R. and O.T. conceived the project and designed the experiments. D.R. constructed the measurement setups, performed the experiments, and analyzed the extracted data. O.B helped in designing the experiment and, together with D.R., fabricated the samples. S.S. and L.K. performed the calculations and participated together with D.R. and O.T. in the overall analysis of the results. D.R. and O.T. wrote the paper and all coauthors commented on the manuscript.

Notes

The authors declare no competing financial interest.

■ ACKNOWLEDGMENTS

D.R. and O.T. are grateful to E. Scheer, F. Striegl, and T. Pietch for their valuable help with the lithography process. O.T. and L. K. thank the Harold Perlman Family for their support and acknowledge funding by the Israel Science Foundation (Grant 089/15). O.T. and L.K. further acknowledge support from the Minerva Foundation (Grant 711136) and the Lise Meitner Minerva Center for Computational Chemistry, respectively.

■ REFERENCES

(1) Wolf, S. A.; Awschalom, D. D.; Buhrman, R. A.; Daughton, J. M.; Von Molnar, S.; Roukes, M. L.; Chtchelkanova, A. Y.; Treger, D. M. *Science* **2001**, *294*, 1488–1495.

(2) Sahoo, S.; Kontos, T.; Furer, J.; Hoffmann, C.; Gräber, M.; Cottet, A.; Schönenberger, C. *Nat. Phys.* **2005**, *1*, 99–102.

DOI: 10.1021/acs.nanolett.5b04674
Nano Lett. 2016, 16, 1741–1745

(3) Loth, S.; Baumann, S.; Lutz, C. P.; Eigler, D. M.; Heinrich, A. J. *Science* **2012**, *335*, 196−199.
(4) Sankey, J. C.; Cui, Y. T.; Sun, J. Z.; Slonczewski, J. C.; Buhrman, R. A.; Ralph, D. C. *Nat. Phys.* **2008**, *4*, 67−71.
(5) Rocha, A. R.; Garcia-Suarez, V. M.; Bailey, S. W.; Lambert, C. J.; Ferrer, J.; Sanvito, S. *Nat. Mater.* **2005**, *4*, 335−339.
(6) Ziegler, M.; Néel, N.; Lazo, C.; Ferriani, P.; Heinze, S.; Kröger, J.; Berndt, R. *New J. Phys.* **2011**, *13*, 085011.
(7) Aradhya, S. V.; Venkataraman, L. *Nat. Nanotechnol.* **2013**, *8*, 399−410.
(8) Raman, K. V.; Kamerbeek, A. M.; Mukherjee, A.; Atodiresei, N.; Sen, T. K.; Lazić, P.; Caciuc, V.; Michel, R.; Stalke, D.; Mandal, S. K.; Blügel, S.; Münzenberg, M.; Moodera, J. S. *Nature* **2013**, *493*, 509−513.
(9) Schmaus, S.; Bagrets, A.; Nahas, Y.; Yamada, T. K.; Bork, A.; Bowen, M.; Beaurepaire, E.; Evers, F.; Wulfhekel, W. *Nat. Nanotechnol.* **2011**, *6*, 185−189.
(10) Li, J. J.; Bai, M. L.; Chen, Z. B.; Zhou, X. S.; Shi, Z.; Zhang, M.; Ding, S.-Y; Hou, S.-M; Schwarzacher, W.; Nichols, R. J.; Mao, B. W. *J. Am. Chem. Soc.* **2015**, *137*, 5923−5929.
(11) McGuire, T.; Potter, R. *IEEE Trans. Magn.* **1975**, *11*, 1018−1038.
(12) Bolotin, K. I.; Kuemmeth, F.; Ralph, D. C. *Phys. Rev. Lett.* **2006**, *97*, 127202.
(13) Keane, Z. K.; Yu, L. H.; Natelson, D. *Appl. Phys. Lett.* **2006**, *88*, 062514.
(14) Velev, J.; Sabirianov, R. F.; Jaswal, S. S.; Tsymbal, E. Y. *Phys. Rev. Lett.* **2005**, *94*, 127203.
(15) Jacob, D.; Fernández-Rossier, J.; Palacios, J. J. *Phys. Rev. B: Condens. Matter Mater. Phys.* **2008**, *77*, 165412.
(16) Häfner, M.; Viljas, J. K.; Cuevas, J. C. *Phys. Rev. B: Condens. Matter Mater. Phys.* **2009**, *79*, 140410.
(17) Barraud, C.; Seneor, P.; Mattana, R.; Fusil, S.; Bouzehouane, K.; Deranlot, C.; Graziosi, P.; Heuso, L.; Bergenti, I.; Dediu, V.; Petroff, F.; Fert, A. *Nat. Phys.* **2010**, *6*, 615−620.
(18) Sanvito, S. *Nat. Phys.* **2010**, *6*, 562−564.
(19) Smogunov, A.; Dappe, Y. J. *Nano Lett.* **2015**, *15*, 3552−3556.
(20) Atodiresei, N.; Brede, J.; Lazić, P.; Caciuc, V.; Hoffmann, G.; Wiesendanger, R.; Blügel, S. *Phys. Rev. Lett.* **2010**, *105*, 066601.
(21) Gabureac, M.; Viret, M.; Ott, F.; Fermon, C. *Phys. Rev. B: Condens. Matter Mater. Phys.* **2004**, *69*, 100401.
(22) Shi, S.-F.; Ralph, D. C. *Nat. Nanotechnol.* **2007**, *2*, 522−523.
(23) Gil, W.; Görlitz, D.; Horisberger, M.; Kötzler, J. *Phys. Rev. B: Condens. Matter Mater. Phys.* **2005**, *72*, 134401.
(24) Leighton, C.; Song, M.; Nogués, J.; Cyrille, M. C.; Schuller, I. K. *J. Appl. Phys.* **2000**, *88*, 344−347.
(25) Egle, S.; Bacca, C.; Pernau, H. F.; Huefner, M.; Hinzke, D.; Nowak, U.; Scheer, E. *Phys. Rev. B: Condens. Matter Mater. Phys.* **2010**, *81*, 134402.
(26) Pauly, F.; Dreher, M.; Viljas, J. K.; Häfner, M.; Cuevas, J. C.; Nielaba, P. *Phys. Rev. B: Condens. Matter Mater. Phys.* **2006**, *74*, 235106.
(27) Untiedt, C.; Dekker, D.M. T.; Djukic, D.; van Ruitenbeek, J. M. *Phys. Rev. B: Condens. Matter Mater. Phys.* **2004**, *69*, 081401.
(28) Yamada, R.; Noguchi, M.; Tada, H. *Appl. Phys. Lett.* **2011**, *98*, 053110.
(29) Kawahara, S. L.; Lagoute, J.; Repain, V.; Chacon, C.; Girard, Y.; Rousset, S.; Smogunov, A.; Barreteau, C. *Nano Lett.* **2012**, *12* (9), 4558−4563.
(30) Yoshida, K.; Hamada, I.; Sakata, S.; Umeno, A.; Tsukada, M.; Hirakawa, K. *Nano Lett.* **2013**, *13* (2), 481−485.
(31) Kiguchi, M.; Tal, O.; Wohlthat, S.; Pauly, F.; Krieger, M.; Djukic, D.; Cuevas, J. C.; van Ruitenbeek, J. M. *Phys. Rev. Lett.* **2008**, *101*, 046801.
(32) Otte, F.; Heinze, S.; Mokrousov, Y. *Phys. Rev. B: Condens. Matter Mater. Phys.* **2015**, *92*, 220411.
(33) Wende, H.; Bernien, M.; Luo, J.; Sorg, C.; Ponpandian, N.; Kurde, J.; Miguel, J.; Piantek, M.; Xu, X.; Eckhold, Ph.; Kuch, W.; Baberschke, K.; Panchmatia, P. M.; Sanyal, B.; Oppeneer, P. M.; Eriksson, O. *Nat. Mater.* **2007**, *6*, 516−520.
(34) Brede, J.; Atodiresei, N.; Kuck, S.; Lazić, P.; Caciuc, V.; Morikawa, Y.; Hoffmann, G.; Blügel, S.; Wiesendanger, R. *Phys. Rev. Lett.* **2010**, *105*, 047204.
(35) Demuth, J. E.; Eastman, D. E. *Phys. Rev. B* **1976**, *13*, 1523−1527.
(36) Yelin, T.; Vardimon, R.; Kuritz, N.; Korytár, R.; Bagrets, A.; Evers, F.; Kronik, L.; Tal, O. *Nano Lett.* **2013**, *13*, 1956−1961.

DOI: 10.1021/acs.nanolett.5b04674
Nano Lett. 2016, 16, 1741−1745

Enhanced magnetoresistance in molecular junctions by geometrical optimization of spin-selective orbital hybridization

Supporting information

David Rakhmilevitch[1], Soumyajit Sarkar[2], Ora Bitton[3], Leeor Kronik[2], and Oren Tal[1]

1. Department of Chemical Physics, Weizmann Institute of Science, Rehovot, Israel
2. Department of Materials and Interfaces, Weizmann Institute of Science, Rehovot, Israel
3. Department of Chemical Research Support, Weizmann Institute of Science, Rehovot, Israel

I. Device fabrication and introduction of molecules.

The break junction samples were fabricated on phosphor-bronze substrates, spin coated with a 2-μm thick dielectric polyimide layer. Contact pads and leads were patterned using photolithography and evaporation of a 10 nm thick chrome layer followed by an 80 nm thick gold layer. The constriction was patterned using e-beam lithography followed by evaporation of an 80 nm thick nickel layer. The polyimide layer below the constriction was under-etched using inductively coupled plasma to form a freely suspended region of about 320 nm. The device was mounted into a vacuum chamber equipped with a three point bending mechanism. All AMR measurements were performed after cooling the chamber to 5.9 K. The constriction was narrowed to form an atomic junction by bending the substrate using a combination of a screw-nut mechanism for rough adjustments and a piezo-element for fine-tuning. AMR measurements were performed using a conventional lock-in current-bias scheme, while a voltage-bias lock-in technique was used for inelastic electron spectroscopy measurements. Benzene molecules (Sigma Aldrich, Anhydrous, 99.8%) were introduced to the junction using a molecular source composed of heated vacuum tube, connecting a benzene reservoir held at room temperature to a funnel right above the junction. The benzene was further purified in-situ by several freeze-pump-thaw cycles before admission of molecules to the junction.

II. The role of magneto-elastic effects

Ferromagnetic metals deform under applied magnetic field, an effect referred to as magnetostriction. Despite this being a rather small effect[1] ($\frac{\Delta l}{l} \sim 10^{-5}$), it was previously shown that nano-contacts, created by electro-deposition or by breaking a macroscopic ferromagnetic wire, can deform by orders of tens of nanometers, resulting in over 1000% variations in conductance across the junction[2]. However, experiments performed on lithographically defined break junctions in which metallic ferromagnetic films are anchored to a rigid substrate, indicated that such deformations can be negligible, allowing the detection of AMR in the order of 10% in agreement with related calculations[3]. This was further verified by demonstrating a clear

suppression of magnetostriction upon reduction of the length of the freely suspended region at the center of a ferromagnetic junction[4].

In order to diminish possible magnetostrictive effects in our experiments, the ferromagnetic section of the junction was constrained to less than 10 μm in length, along the junction axis. More importantly, the freely suspended region was reduced to less than 300 nm, as described in section I. The insignificant role of magnetostriction in our measurements was verified by several independent observations:

(1) Magneto-conductance measurements taken in the tunneling regime after breaking the contact and before the introduction of molecules did not exhibit any systematic change in conductance (Fig. S1a). This observation is in contrast to the expected high sensitivity of conductance in the tunneling regime to magnetostriction-induced variations in the distance between the electrodes of the examined junctions.

(2) The conductance response of our Ni atomic junctions to magnetic field applied in parallel and perpendicular to the junction has comparable amplitude (Fig. S3), suggesting that longitudinal deformations play a minor role.

(3) Magneto-conductance measurements in the single atom contact regime resulted in a conductance change of less than 10% (Fig. S1b), which is comparable to results, obtained previously on both Ni atomic contacts without a freely suspended region[5] and permalloy atomic contacts[6].

(4) Following the introduction of molecules to the Ni junction, we measured a non-monotonic magneto-conductance trend in response to junction elongation (Fig. 3b of the main text). This observation is consistent with negligible magnetostriction contribution. This is because the latter is expected to yield a monotonic increase in the magneto-conductance ratio as

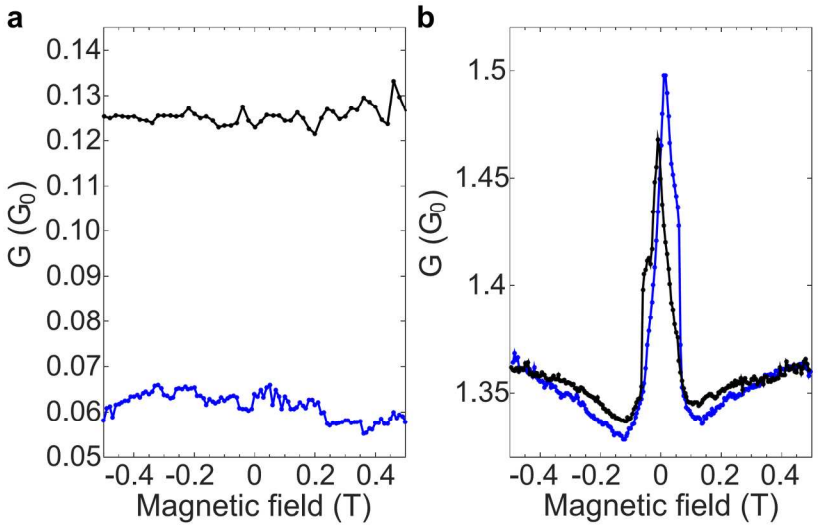

Figure S1: Magnetoconductance of Ni junctions measured in the tunneling regime (a) and in the atomic contact regime (b). The measurements were taken on different junctions.

the conductance is reduced towards the tunneling regime and the conductance sensitivity to interelectrode distance is increased.

III. AMR measurements in a rotating magnetic field.

To establish the AMR origin of the observed change in conductance with magnetic field, conductance measurements were performed while rotating a magnetic field of 0.3 T in the plane of the junction (See Fig. S2a). The chosen magnetic field amplitude is above the field required to saturate the magnetization of the electrodes. This measurement scheme is less appealing since itis susceptible to sharp variations in the measured conductance, possibly due to atomic rearrangements[7]. Figure S2b presents the conductance of an atomic junction as a function of magnetic field angle relative to the junction axis. The overall changes in conductance are in agreement with the measured values obtained by sweeping the field along the axis. However, in contrast to the latter measurement scheme, abrupt conductance variations can be observed in Fig. S2b, leading to a less reliable determination of the magneto-conductance amplitude.

Figure S2c presents the measured conductance for two independent Ni/benzene molecular junctions, exhibiting an increase in conductance when the field is directed at an angle of $45<\theta<135$ with respect to the junction axis. This angular dependence points to an AMR origin for the observed behavior, excluding other origins such as tunneling magnetoresistance**.**

IV. Determination of the easy axis of the junction.

The easy axis of the junction was determined from the conductance response of the junction to a magnetic field applied in different directions[8] as presented in Fig. S3. When the magnetic field

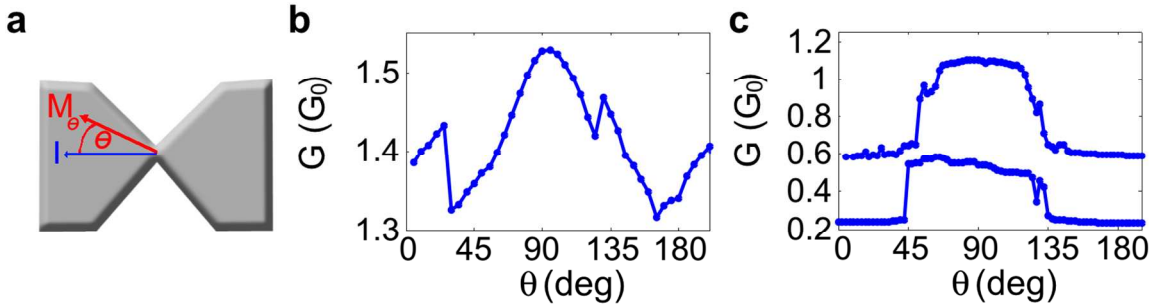

Figure S2: Conductance measurements as a function of a rotating magnetic field. (a) Schematic illustration of the relative direction of magnetization and current during the measurement. Measurements of magneto-conductance of a Ni atomic junction (b) and two different realizations of molecular junctions (c).

was swept either along the junction axis (z axis; Fig. S3a) or out of the junction plane (y axis; Fig. S3b), conductance variations in the order of 7% were observed, in agreement with previously reported results5. The conductance response to a magnetic field in the plane of the junction and perpendicular to its axis (x axis; Fig. S3c) exhibited a different behavior. In contrast to the monotonic change of conductance as the magnetic field was increased along the z or the y axis, during this measurement the conductance was rather insensitive to the applied magnetic field with minor features near zero magnetic field. This behavior is consistent with spontaneous magnetization of the junction along the x direction[9]. Applying a magnetic field in this direction preserves the perpendicular orientation of magnetization with respect to the current throughout the measurement, except near zero magnetic field where the magnetization switching occurs. Since the angle between the magnetization and the current does not vary, no systematic changes in the conductance are expected, as indeed seen in Fig. S3c. While shape anisotropy can lead to an easy axis along the z axis, we assign the observed orientation of spontaneous magnetization to the stress applied on the ferromagnetic film due to the breaking process. We note that a transverse in-plane spontaneous magnetization of a Ni thin film of a similar width under tensile stress was also shown previously[10].

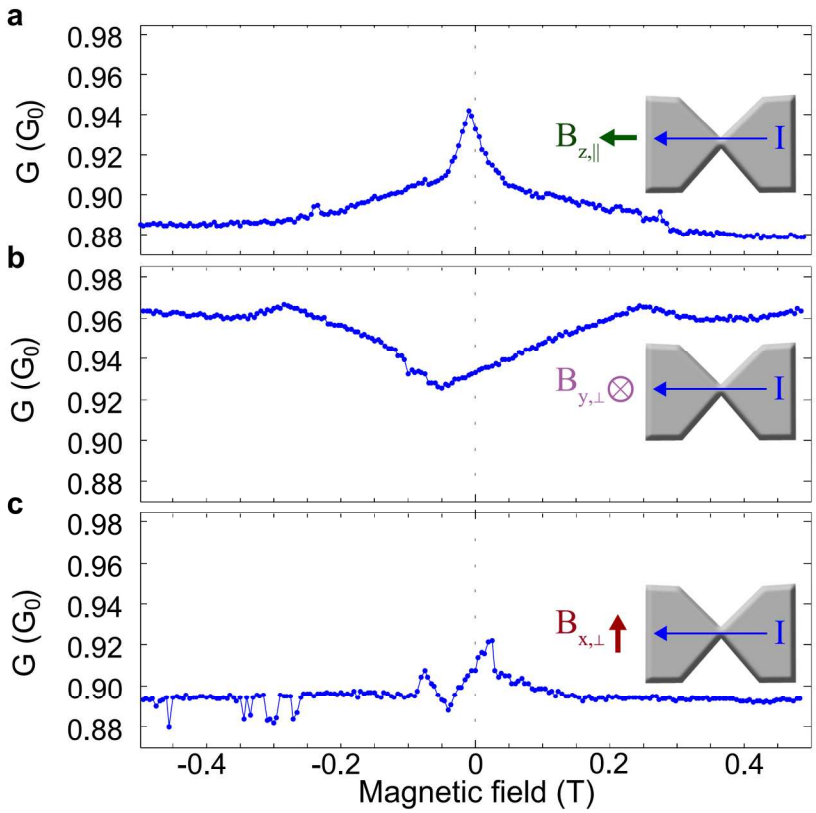

Figure S3: Conductance measurements as a function of magnetic field along the three axes of the junction as defined in the insets. The measurements were performed for Ni\benzene junctions in a stable, compact configuration.

V. Establishing transport through the molecule using inelastic electron spectroscopy:

In order to verify that the introduction of benzene to the Ni sample indeed formed molecular junctions, we performed inelastic electron tunneling spectroscopy (IETS) to look for the signature of molecular-junction vibrations. Figure S4 presents an example for the measured normalized IETS signal before and after the introduction of molecules. The feature around zero-bias observed in both graphs is attributed to excitation of phonons and magnons in the metallic electrodes[11], on top of energy-dependent variations in the electronic density of states of the point contact. However, after the introduction of molecules we observed IETS peaks around a bias voltage of 53 ± 3 mV. Similar features were previously shown to arise from vibration-induced electron scattering in benzene-based molecular junctions[12,13,14].

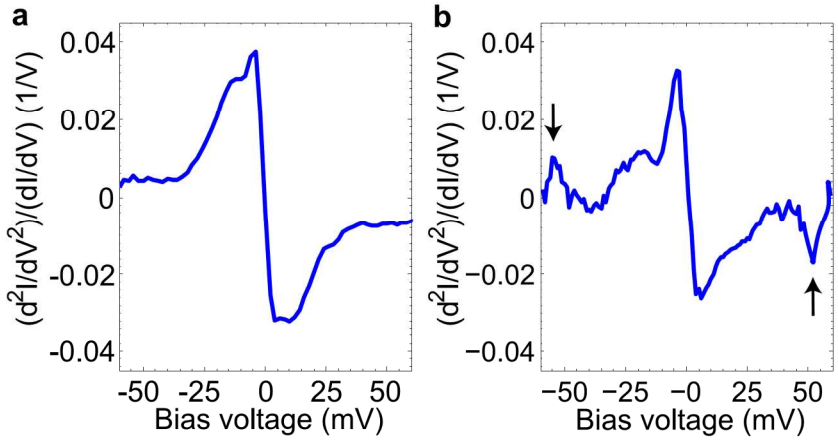

Figure S4: Differential conductance measurements taken on a Ni atomic junction before (a) and after (b) the introduction of molecules. Arrows indicate the onset voltage for vibration activation.

VI. Effects of variable molecular configurations.

The multitude of different metal-molecule configurations suggests some inherent variability in the magneto-transport properties of the junctions. Out of the 43 junctions we examined, 6 exhibited magnetoresistance higher than 150%, while the average magnetoresistance value was 58.9%. This means that while configurations with extremely high AMR are robust and reproducible they occur less often.

The effect of the molecular configuration on the measured AMR is even more evident when examining the influence of junction elongation, as exemplified by the non-monotonic AMR response in Figure 3 in the main text. Such non-monotonic behavior was observed in about 60% of the successfully-elongated junctions, some of which are shown in figure S5.

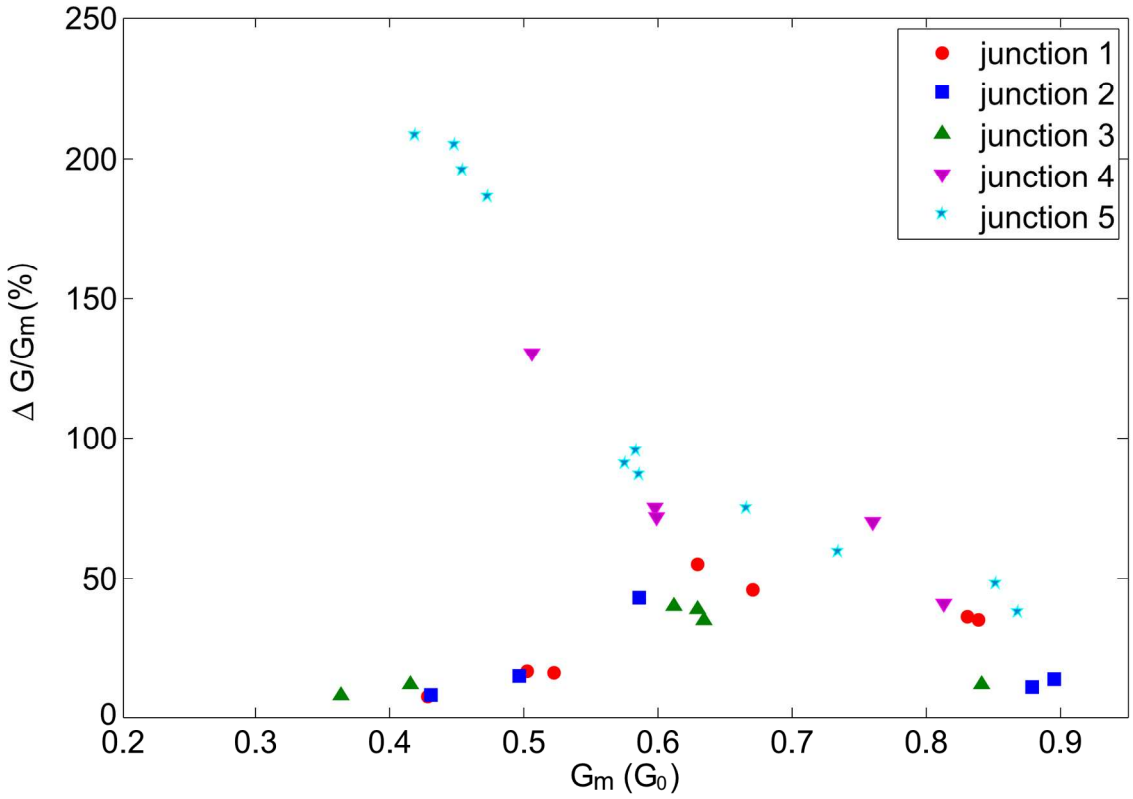

Figure S5: The dependence of AMR on junction elongation for different Ni-benzene junctions.

The monotonic behavior of other junctions (such as junctions 4 and 5) may result from premature breaking of the junction during the elongation process before the extended configurations were reached.

VII. Computational Methodology

All calculations were carried out within the framework of density functional theory (DFT)[15], using the generalized –gradient approximation of Perdew, Burke, and Ernzerhof (PBE)[16]. All work has been performed using the VASP plane wave code[17], with a plane wave cut off energy of 550eV. Ion-electron interaction was treated by means of the projector augmented wave method[18,19]. Fermi-Dirac occupation "smearing" over an energy equivalent to 20meV was used to accelerate convergence. An orthogonal super-cell of dimensions 24x24x48 $Å^3$, with single k-point sampling, was used throughout. This allows for the description of a finite system despite the periodic boundary condition as it affords a vacuum of ~10-12 Å between system images, which was found to be sufficient for keeping spurious interactions between system replicas at a negligible level. Geometry optimization was performed until all force components were smaller than $5x10^{-3}$ eV/Å.

VIII. Details of the Model System

The computed model system consisted of two Ni electrodes, oriented along the (111) direction of a face-centered cubic (FCC) lattice and bridged by a benzene molecule, as shown in Fig. S6. Convergence with the number of atomic Ni planes, *n,* was explicitly verified, with *n*=5 used. Junction elongation was simulated by varying the electrode separation while keeping the unit cell dimension constant. Electrode separation was defined as the normal distance between the planes containing the three atoms located immediately behind the apex atom of each electrode. The positions of the apex Ni atoms and the atoms forming the benzene molecule were then optimized without symmetry constraints. Electrode separation was varied between 6.8 Å and 8.3 Å. We found that a separation of 7.2 Å is the lowest energy configuration. At the lowest energy separation, the benzene molecule was found to be normal to the inter-electrode axis. For inter electrode separation beyond 7.5 Å, tilting from the position was increasingly observed.

IX. Charge transfer between molecule and electrodes

We computed the *z* (inter-electrode axis)-distribution of the *xy*-averaged valence charge density difference between one Ni-electrode with the benzene molecule, $\rho_{Elec}(x,y,z)$, and the benzene molecule alone, $\rho_B(x,y,z)$, in the form: $\rho_d(z) = \iint_{-\infty}^{\infty}(\rho_{Elec}(x,y,z) - \rho_B(x,y,z))\,dx\,dy$[20], as a function of the distance along the axis of the electrode. The integration limits were set to the end points of the unit cell along the *x* and *y* directions. The result is shown in Fig. S7. For each atomic layer of the electrode, a peak at the corresponding *z* coordinate value is observed. The benzene molecule plane is at a distance of 19 Å along the *z* axis and shows no significant signature of charge density difference. Because the PBE exchange-correlation functional used here typically overestimates charge transfer[21], these results can be viewed as an upper bound charge, which means that charge transfer from electrode to molecule can be ruled out for all practical purposes.

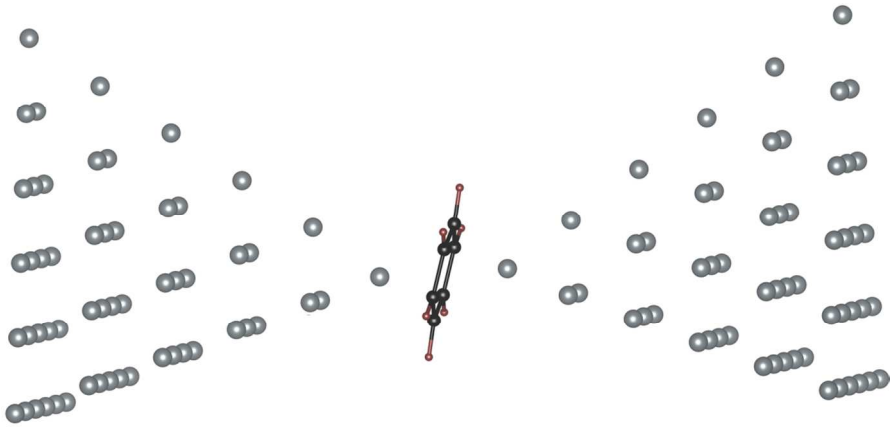

Figure S6: Schematic diagram of the model system used in the computational work.

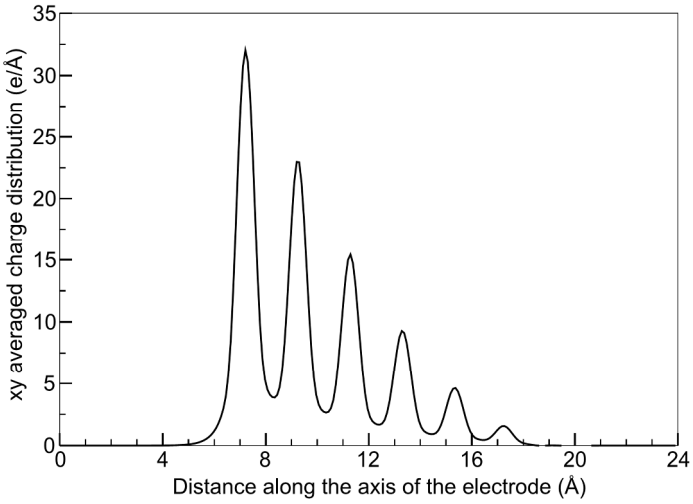

Figure S7: Plane-averaged valence charge density difference as a function of distance along the electrode axis.

X. Real-space plot of the spin-resolved charge density

The real space distribution of charge density, obtained from states residing within an "energy window" of 100 meV around the Fermi energy is plotted for up spin channel in Fig. S8, with an iso-surface value of 0.001 eÅ^{-3}, which is much lower than that used in the main text – 0.007 eÅ^{-3}. At this very low iso-surface value, one can see some contribution at the benzene molecule. But, interestingly, the charge density resembles σ states more than π states. This further makes the point of spin-selective electron transport, because the spin-polarized π states, discussed in the main text as supporting transport, are in the down-spin channel.

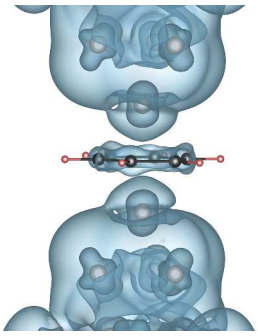

Figure S8: Charge density distribution in real space, collected from orbitals within an energy window of 100 meV around the Fermi energy for the spin-up channel, based on a calculation at equilibrium tip separation of 7.2 Å.

References

[1]Cullity, B. D., Graham, C.D, *Introduction to Magnetic Materials* (Wiley, New jersey 2009).

[2]Egelhoff, W.F. *et. al.,* Artifacts that mimic ballistic magnetoresistance*. J. Magn. Magn.Mater.*, **287**. 496 (2005).

[3]Häfner, M., Viljas, J. K., and Cuevas, J. C., Theory of anisotropic magnetoresistance in atomic-sized ferromagnetic metal contacts. *Phys. Rev. B,* **79**, 140410 (2009).

[4]Gabureac, M., Viret, M., Ott, F., and Fermon, C., Magnetoresistance in nanocontacts induced by Magnetostrictive effects. *Phys. Rev. B*, **69**, 100401 (2004).

[5]Keane, Z. K., Yu, L. H., and Natelson, D., Magnetoresistance of atomic-scale electromigrated nickel nanocontacts. *Appl. Phys. Lett.,* **88**, 062514 (2006).

[6]Bolotin, K. I., Kuemmeth, F. and Ralph, D. C., Anisotropic Magnetoresistance and Anisotropic Tunneling Magnetoresistance due to Quantum Interference in Ferromagnetic Metal Break Junctions. *Phys. Rev. Lett.,* **97**, 127202 (2006).

[7]Shi, S.-F., Bolotin, K. I., Kuemmeth, F., and Ralph, D. C., Temperature dependence of anisotropic magnetoresistance and atomic rearrangements in ferromagnetic metal break junctions. *Phys. Rev. B*, **76**, 184438 (2007).

[8]Giddings, A. D. *et. al.,* Large Tunneling Anisotropic Magnetoresistance in (Ga,Mn)As Nanoconstrictions. *Phys. Rev. Lett.* **94**, 127202 (2005).

[9]Vila, L., Piraux, L., George, J. M., and Faini, G., Multiprobe magnetoresistance measurements on isolated magnetic nanowires. *Appl. Phys. Lett.,* **80**, 3805 (2002).

[10]Weileret, M. *et al.*, Voltage controlled inversion of magnetic anisotropy in a ferromagnetic thin film at room temperature, New J. of Phys., **11**, 013021(2009).

[11]Naidyuk, Y. G. and Yanson, I. K., *Point-contact spectroscopy*, vol. 145, (Springer, 2005).

[12]Kiguchi, M., *et. al.* Highly Conductive Molecular Junctions Based on Direct Binding of Benzene to Platinum Electrodes. *Phys. Rev. Lett.,* **101**, 046801 (2008).

[13]Kaneko, S., Nakazumi, T., and Kiguchi, M., Fabrication of a Well-Defined Single Benzene Molecule Junction Using Ag Electrodes. *J. Phys. Chem. Lett.,***1**, 3520 (2010).

[14]Stipe, B. C., Rezaei, M. A., and Ho, W., Single-Molecule Vibrational Spectroscopy and Microscopy. *Science,* **280**, 1732 (1998).

[15]Parr, R. G., and Yang, W., *Density-Functional Theory of Atoms and Molecules,* (Oxford University Press, 1989).

[16]Perdew, J. P., Burke, K., and Ernzerhof, M., Generalized Gradient Approximation Made Simple. *Phys. Rev. Lett.***77**, 3865 (1996).

[17]Kresse, G., and Furthmüller, J., Efficient iterative schemes for *ab initio* total-energy calculations using a plane-wave basis set. *Phys. Rev. B*, **54**, 11169 (1996).

[18]Blöchl, P. E., Projector augmented-wave method. *Phys. Rev. B,* **50**, 17953 (1994).

[19]Kresse, G.,and Joubert, D., From ultra-soft pseudopotentials to the projector augmented-wave method. *Phys. Rev. B,* **59**, 1758 (1999).

[20]Deutsch, D., Natan, A., Shapira, Y., and Kronik, L., Electrostatic Properties of Adsorbed Polar Molecules: Opposite Behaviour of a Single Molecule and a Molecular Monolayer. *J. Am. Chem. Soc.,* **129**, 989 (2007).

[21]Kümmel, S., and Kronik, L., Orbital-dependent density functionals: Theory and applications. *Rev. Mod. Phys.***, 80**, 3 (2008).